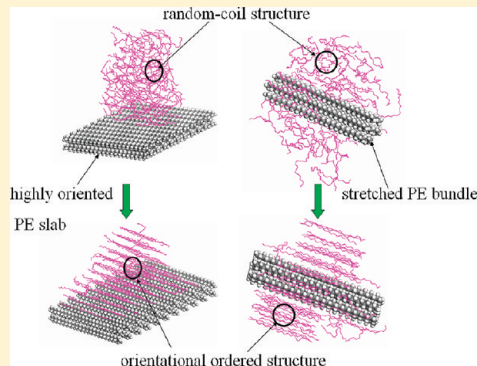


# Isothermal Crystallization of Short Polymer Chains Induced by the Oriented Slab and the Stretched Bundle of Polymer: A Molecular Dynamics Simulation

Jun-Sheng Yang, Chuan-Lu Yang,\* Mei-Shan Wang, Bao-Dong Chen, and Xiao-Guang Ma

School of Physics, Ludong University, Yantai 264025, People's Republic of China

**ABSTRACT:** Information on the interfacial interaction is vital in understanding the crystallization of short polymer chains around oriented nuclei. However, this interaction is difficult to observe at the atomic level. Molecular dynamics simulations are performed to investigate the structural formation of polymer chains induced by the highly oriented slab or the stretched bundle of polymer chains. The results show that the surface-induced crystallization of polymer chains is greatly influenced by the foreign surface on the crystal structure and the morphology of the polymers, hence providing molecular-level support for previous experimental observations [Lotz et al. *Macromolecules* 1993, 26, 5915 and Yan et al. *Macromolecules* 2009, 42, 9321]. The order parameter  $S$  and the configurations show that the ability of the polypropylene (PP) slab to induce the polyethylene (PE) melt crystallization is weaker than that of the PE slab and that the short PE chains display multiple orientations on the PP slab. In addition, the crystallization rate was found to be dependent on the lattice matching between the free chains and the substrates on the contact lattice planes.



## I. INTRODUCTION

Polymer crystallization controls the structural formation processes and final properties of polymer materials, including the mechanical properties, glass transition temperature, and molecular mobility.<sup>1–3</sup> The process is a transition from a randomly coiled to perfectly ordered state. Recently, surface-induced polymer crystallization has attracted great attention in material science, because the key factors in tailoring the properties of polymers, namely, the crystal structure and morphology of the polymers, are dependent on the foreign surface.<sup>4–7</sup> Therefore, we need to know much more about the molecular mechanism of the surface-induced polymer crystallization.

In polymer epitaxy, foreign surfaces have multifarious influences on the polymer crystallization, depending on the surface morphology, the polymer used, and the interaction between the substrate and the polymer melt. The indirect evidence for this was reported by Jiang et al.<sup>8</sup> They found that the perylo[1,12-*b,c,d*]thiophene (PTH) can grow epitaxially on the highly oriented polyethylene (PE) substrate and form lathlike crystals, thus allowing the fabrication of large well-arranged PTH films with a unique crystalline structure. Lotz et al.<sup>9,10</sup> successfully modulated the melt-crystallization process of isotactic poly(1-butene) in different modifications by regulating the crystalline structure of polymer substrates. The epitaxial growth mechanism is generally based on the structural similarity between the substrate and overgrowth materials in the contact lattice planes. Therefore, lattice matching should play a dominant role in surface-induced polymer crystallization.

The physical and chemical properties of polymeric materials can be easily tailored by nanoparticles at different scales. The effect of nanoparticle dimensionality on the polymer crystallization was discussed by Xu et al.<sup>11</sup> They found that low-dimensional nanoparticles greatly induce polymer crystallization. The differences in the induction abilities of one-dimensional (1-D) carbon nanotubes (CNTs) and two-dimensional (2-D) graphene nanosheets (GNSs) are discussed in our previous simulation study.<sup>12</sup> Moreover, our simulation results show that the inductive ability of 1-D CNTs is stronger than that of 2-D GNSs. For fiber-reinforced polymer systems, induced polymer crystallization on fiber surfaces is also an unavoidable phenomenon. However, this observation is still constantly debated in academic circles. Thus, molecular dynamics (MD) simulation can also be a power tool in investigating polymer crystallization on outer surfaces to provide molecular-level support for the experimental hypothesis.

Flow-induced polymer crystallization has been investigated.<sup>13,14</sup> During the process, chains longer than the critical length would stretch and form the shish, whereas the shorter chains would not stretch but form folded chain lamellae, the kebabs. For the polymer blends of the long and short chains, Balzano et al.<sup>15</sup> and Hsiao et al.<sup>16</sup> confirmed that the long chains are the major component of the oriented nuclei. Both groups investigated the blends of the long and short chains and

Received: October 1, 2011

Revised: January 11, 2012

Published: January 12, 2012

found that the long chains had a higher “effective” melting temperature. On the basis of the results of Balzano et al.<sup>15</sup> and Hsiao et al.,<sup>16</sup> Li et al.<sup>17</sup> showed that the long chains can be the main contributor of the oriented nuclei during the flow-induced polymer crystallization. Recently, the simulation results of Hu et al.<sup>18</sup> showed that a single aligned chain can act as a “template” or shish for polymer epitaxy or the crystallization of the kebab without flow. However, it is too simple that only one chain is stretched in the flow-induced crystallization. The rational model is that the oriented slab or stretched bundle of polymer chains plays the role of the oriented nuclei. The present paper demonstrates the mechanisms of the structural formation of polymers by different substrates, particularly the bundle of polymer chains, at the molecular level. The effect of the structural similarity between the polymers and the inducing unit (IU) on the crystal structure of the polymers is also given enough attention.

## II. MODEL AND SIMULATION METHOD

For the present computational model of the polymer chain, the single PE chain is composed of 20 CH<sub>x</sub> groups to allow for fast simulation. Initially, 120 PE chains are randomly distributed on a highly oriented ordered IU surface. Two kinds of IU surfaces are used in our computational model, namely, the polymer slab and bundle. The polymer-slab surfaces include a two-layered oriented PE slab (PES) or polypropylene (PP) slab (PPS). For the polymer bundle, the PE bundle (PEB) includes seven chains and the PP bundle (PPB) has three chains. To confirm that the PE chains have completely relaxed, we perform MD simulations for 300 ps at a high temperature ( $T = 700$  K), which is then reduced to a lower value ( $T = 450$  K). The latter is possibly the crystallization temperature according to previous literature.<sup>19</sup> Figure 1 shows the initial randomly distributed configurations of the PE melt on the highly oriented ordered IU surface. To observe the spatial arrangement of PE chains clearly, we eliminated the hydrogen atoms in the image. However, they were retained in the calculations.

The MD simulations were performed with the Discover module in Materials Studio,<sup>20</sup> and Condensed-phase Optimized Molecular Potentials for Atomistic Simulation Studies (COMPASS) was used as the atomic force field.<sup>21</sup> The COMPASS force field has been successfully used in previous investigations of organic and inorganic materials.<sup>22,23</sup> We have also used the COMPASS force field to simulate the interactions between PE/PP/PS/PPA/PPV and the SWCNT.<sup>24</sup> The force field potential can be represented as<sup>25</sup>

$$E_{\text{total}} = E_{\text{valence}} + E_{\text{cross-term}} + E_{\text{nonbond}} \quad (1)$$

where  $E_{\text{valence}}$  is the valence energy,  $E_{\text{cross-term}}$  is the cross-term interacting energy, and  $E_{\text{nonbond}}$  is the nonbond interacting energy. Each term is detailed as follows:

$$\begin{aligned} E_{\text{valence}} = & \sum_b [K_2(b - b_0)^2 + K_3(b - b_0)^3 + K_4(b - b_0)^4] \\ & + \sum_\theta [H_2(\theta - \theta_0)^2 + H_3(\theta - \theta_0)^3 + H_4(\theta - \theta_0)^4] \\ & + \sum_\phi [V_1[1 - \cos(\phi - \phi_1^0)] + V_2[1 - \cos(2\phi - \phi_2^0)] \\ & + V_3[1 - \cos(3\phi - \phi_3^0)] + \sum_\chi K_\chi \chi^2 + E_{\text{UB}}] \end{aligned} \quad (2)$$

$$\begin{aligned} E_{\text{cross-term}} = & \sum_b \sum_{b'} F_{bb'}(b - b_0)(b' - b'_0) \\ & + \sum_\theta \sum_{\theta'} F_{\theta\theta'}(\theta - \theta_0)(\theta' - \theta'_0) \\ & + \sum_b \sum_\theta F_{b\theta}(b - b_0)(\theta - \theta_0) \\ & + \sum_b \sum_\phi F_{b\phi}(b - b_0)[V_1 \cos \phi + V_2 \cos 2\phi \\ & + V_3 \cos 3\phi] + \sum_{b'} \sum_\phi F_{b'\phi}(b' - b'_0)(b' - b'_0) \\ & \times [F_1 \cos \phi + F_2 \cos 2\phi + F_3 \cos 3\phi] \\ & + \sum_\theta \sum_\phi F_{\theta\phi}(\theta - \theta_0)[V_1 \cos \phi + V_2 \cos 2\phi \\ & + V_3 \cos 3\phi] + \sum_\phi \sum_\theta \sum_{\theta'} K_{\phi\theta\theta'} \cos \phi(\theta - \theta_0) \\ & \times (\theta' - \theta'_0) \end{aligned} \quad (3)$$

$$E_{\text{nonbond}} = \sum_{i>j} \left[ \frac{A_{ij}}{r_{ij}} - \frac{B_{ij}}{r_{ij}^6} \right] + \sum_{i>j} \frac{q_i q_j}{\epsilon r_{ij}} \quad (4)$$

where  $b$  and  $b'$  are the bond lengths,  $\theta$  is the two-bond angle,  $\phi$  is the dihedral torsion angle,  $\chi$  is the out-of-plane angle,  $q$  is the atomic charge,  $\epsilon$  is the dielectric constant, and  $r_{ij}$  is the  $i-j$  atomic separation distance.  $b_0$ ,  $K_i$  ( $i = 2-4$ ),  $\theta_0$ ,  $H_i$  ( $i = 2-4$ ),  $\phi_i^0$  ( $i = 2-4$ ),  $V_i$  ( $i = 1-3$ ),  $F_{bb'}$ ,  $b_0'$ ,  $F_{\theta\theta'}$ ,  $\theta_0'$ ,  $F_{b\theta}$ ,  $F_{b\phi}$ ,  $F_{b'\theta}$ ,  $F_i$  ( $i = 1-3$ ),  $F_{\theta\phi}$ ,  $K_{\phi\theta\theta'}$ ,  $A_{ij}$ , and  $B_{ij}$  are the system-dependent parameters implemented into the Discover module of Materials Studio. In the present simulations, the NVT ensemble with undefined boundary conditions is used and the time step is 1 fs. The Anderson method is applied to control the temperature of the system.<sup>26,27</sup> The cutoff distance is 9.5 Å.

## III. RESULTS AND DISCUSSION

### 3.1. Crystallization of Polymers Induced by the Oriented Polymer Slab

**Experimentally,** the oriented polymer slab that induces the polymer epitaxy can lead to the formation of a unique crystalline structure and the morphology of polymers.<sup>28,29</sup> For example, Yan et al. investigated the crystallization behavior of the poly(butylene adipate) (PBA) solution and the melting process on the highly oriented PES and PPS.<sup>30,31</sup> Their results show that the PBA can crystallize epitaxially on the oriented PE and PP surfaces. To monitor the surface-induced polymer crystallization, we performed dynamics simulations of the structural formation of polymer chains from the amorphous melt phase to the orientational ordered structure. The simulations display the nucleation and growth process of the polymer melt induced by the polymer slab. The MD simulations provide a theoretical understanding of the epitaxial growth mechanism at the molecular level. The epitaxial growth mechanism is generally based on the structural similarity between the substrate and the overgrowth materials in the contact lattice planes.

Figures 2 and 3 show the crystallization behavior of the PE chains on the PES and PPS. Initially, the PE chains are randomly distributed on the slab (Figure 1a). Figure 2 shows that the highly orientational ordered structure can be formed on the PES, indicating that the oriented PES can induce PE-melt crystallization and that the PE chains are primarily parallel to the direction of the PES crystals. Moreover, the PE-melt crystallization on the PES signifies that the oriented PES determines the orientation of the crystallization for all other PE chains and the perfect lattice matching between the short PE

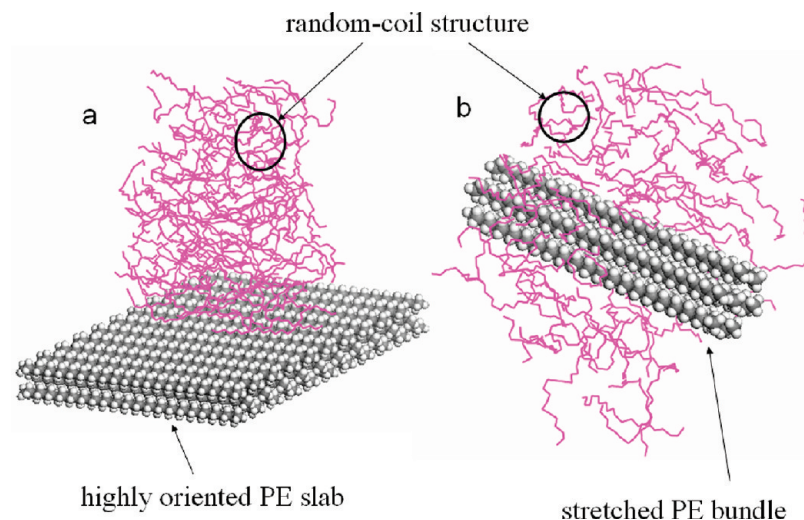


**Figure 1.** Initial molecular model of PE/PES and PE/PEB systems.

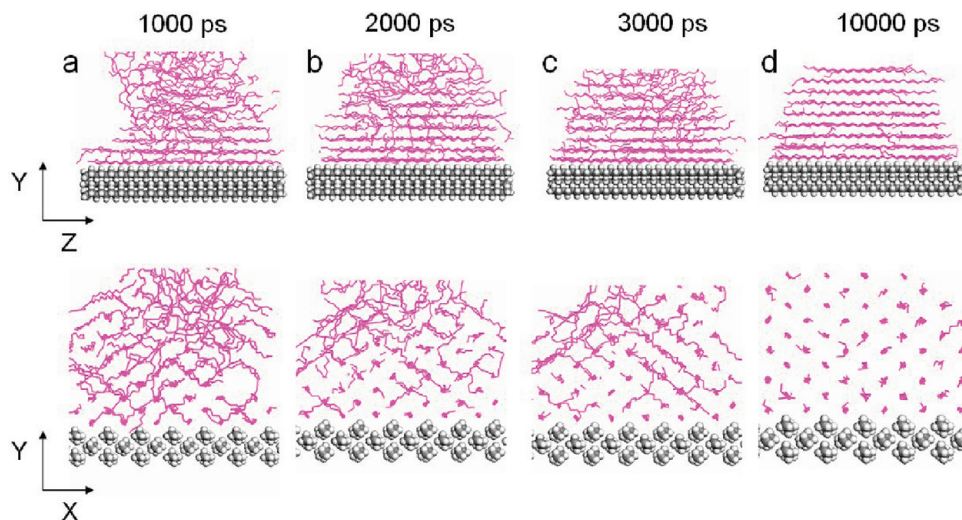


**Figure 2.** Snapshots of the atomic configurations of the PE melts induced by the oriented PES.

melts and the PES. Figure 3 demonstrates that the highly orientational ordered structure can also be formed on the oriented PPS, implying that the oriented PPS also has the ability to induce PE-melt crystallization. We also find that the PE chains have multiple orientations on the PPS and that the PE chains need more time to adjust their configuration. In the PES-induced PE-melt crystallization, the PE chains have exactly the same crystalline structure as that of the PES. On the other hand, in the PPS-induced PE-melt crystallization, the crystalline structure of the PE is different from that of the crystalline PE. The experimental results prove that the most important part of the surface-induced crystallization is attributed to the influence of the foreign surface on the crystalline structure and morphology of polymers.<sup>5,32</sup> Figure 4 shows the time evolution of the total potential and nonbond energies of polymers. As shown, the total potential energy decreases because of the significant decrease of the nonbond energy during crystallization. However, both the nonbond and the total potential energies of the systems show insignificant changes from 5 to 10 ns, implying that the simulation time is long enough for our systems to reach equilibrium.

To rationalize the mechanism of the PE-melt crystallization induced by the PES and PPS, we calculate the bond-

orientational order parameter  $S$  of the singlet layer, which is defined as follows:

$$S = \frac{1}{N(n-2)} \sum_{m=1}^N \sum_{i=3}^n \frac{3 \cos^2 \psi_i^m - 1}{2} \quad (5)$$

where  $N$  and  $n$  are the number of PE chains per layer and the number of  $\text{CH}_x$  groups per PE chain, respectively.  $\psi_i^m$  is the angle between the subbond vector  $b_i^m$  in the slab [ $z, z + dz$ ] and  $z$ .  $z$  is the direction of the PE folded lamellae. The value range of the  $S$  value is  $[-0.5, 1.0]$ , which describes the different levels of orientation. For example, the  $S$  values of 1.0 and  $-0.5$  for the subbonds in the slab [ $z, z + dz$ ] correspond to the chain perfectly parallel or perpendicular to the  $z$ -axis, respectively, while the other  $S$  values correspond to the different arrangements of the chains and all the distributions of the chains are random.

Figure 5 shows the  $S$  values of the PE chains of the first three layers versus time. The value of  $S$  is close to  $-0.25$ , indicating that the PE chains are randomly distributed on the oriented PES and PPS at  $t = 1$  ps. Over time, the value of  $S$  for the PES increases until  $t = 1000$  ps (see Figure 5a). For the PPS, the value of  $S$  remains close to zero until  $t = 3000$  ps, indicating

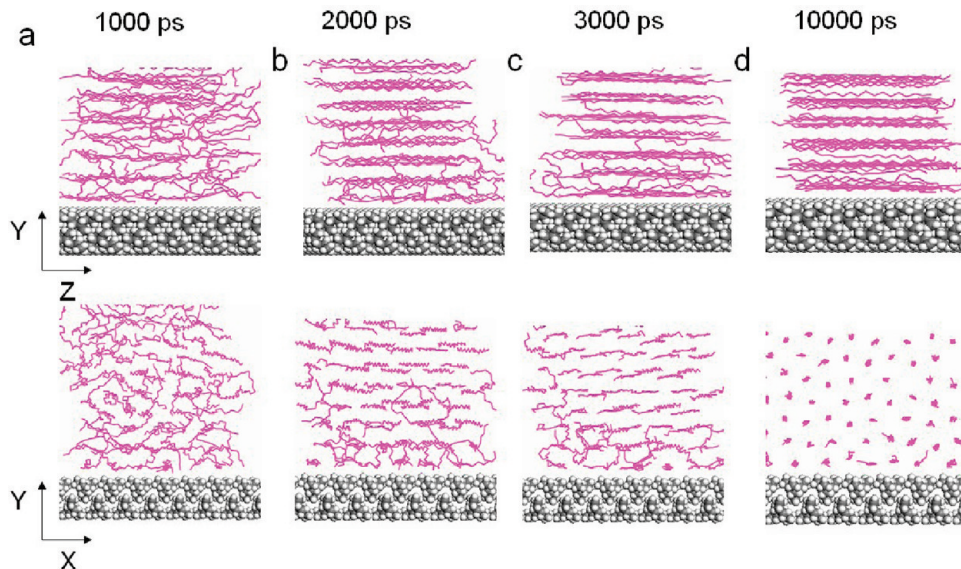


**Figure 3.** Snapshots of the atomic configurations of PE melts induced by the oriented PPS.

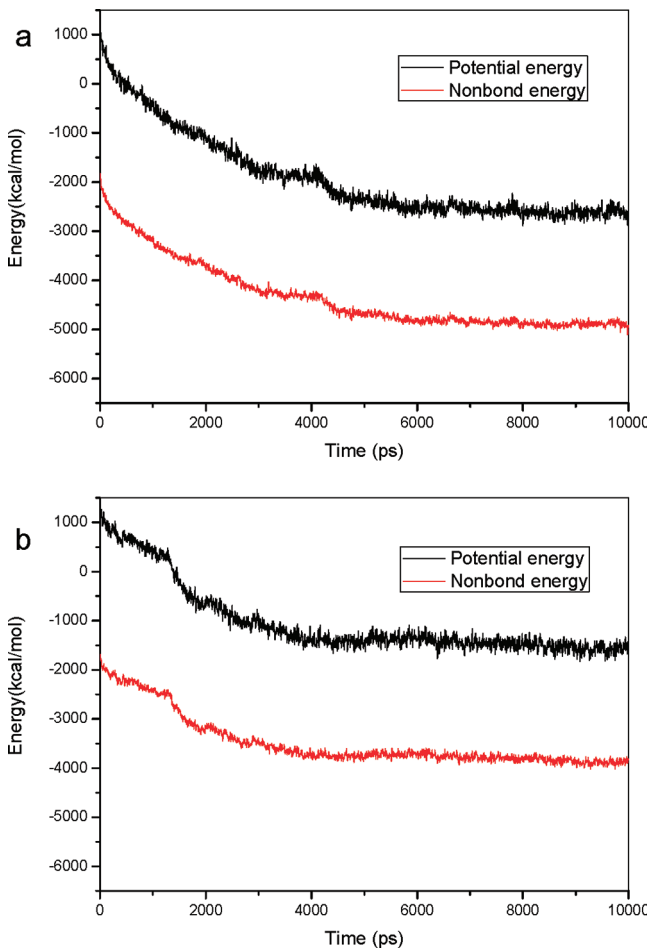


**Figure 4.** Time evolution of nonbond and total potential energies: (a) PE/PES and (b) PE/PPS systems.

that the highly oriented PES has a stronger ability to induce the PE melt crystallization than the PPS. By combining the atomic configurations of the PE chains, we find that the PE chains have multiple orientations on the PPS surface and that the random PE chains need more time to adjust their configuration on the PPS. For the PE/PES system,  $S$  is close to 0.82 at  $t = 10\,000$  ps,

whereas, for the PE/PPS system,  $S$  is close to 0.75 at  $t = 10\,000$  ps. These results imply that the PE chains have multiple orientations on the PPS surface. The surface of the polymer slab is an important factor for the crystallization, the similar crystal structure between the polymer melts, and the polymer slab corresponding to the high  $S$  value.

The MD simulation of the polymer crystallization induced by the polymer slab shows that the outer surface is very important to the crystalline structure and morphology of polymers. The highly oriented PES has a stronger ability to induce PE-melt crystallization than the PPS. By analyzing the value of  $S$  and by observing the configurations, we find that the PE chains are primarily parallel to the direction of the substrate and that the first layer determines the orientation of the crystallization for all other PE chains on the PES. In contrast, the PE chains show multiple orientations on the PPS, and the PE chains need more time to adjust their configurations.

**3.2. Crystallization of Polymers Induced by the Stretched Polymer Bundle.** Polymer crystallization in the extensional flow has a significant influence on polymer processing and the final properties of polymer products. For the blends of the long and short chains, Balzano et al.<sup>15</sup> and Hsiao et al.<sup>16</sup> confirmed that the long chains have a higher “effective” melting temperature. On the basis of the results of Balzano et al.<sup>15</sup> and Hsiao et al.,<sup>16</sup> Li et al.<sup>17</sup> showed that the long chains can be the main contributor of the oriented nuclei during the flow-induced polymer crystallization. History dependence suggests that chains longer than the critical length will stretch and form the shish (the stretched polymer bundle), whereas the shorter chains will not stretch but form the folded chain lamellae, the kebabs. Therefore, we focus on the polymer crystallization induced by the different bundles.

Figure 6 shows the snapshots of the atomic configurations of the PE melts induced by the stretched PEB during isothermal crystallization at 450 K. Similar to the polymer slab that induces polymer crystallization, initially, the polymer chains are randomly distributed around the bundle (Figure 1b). Over time, the highly oriented structure forms on the surface of the stretched chains. Our result corresponds well with the recent report from Li et al.<sup>17</sup> Our result also confirms that the stretched bundle of polymer chains can act as a “template” or

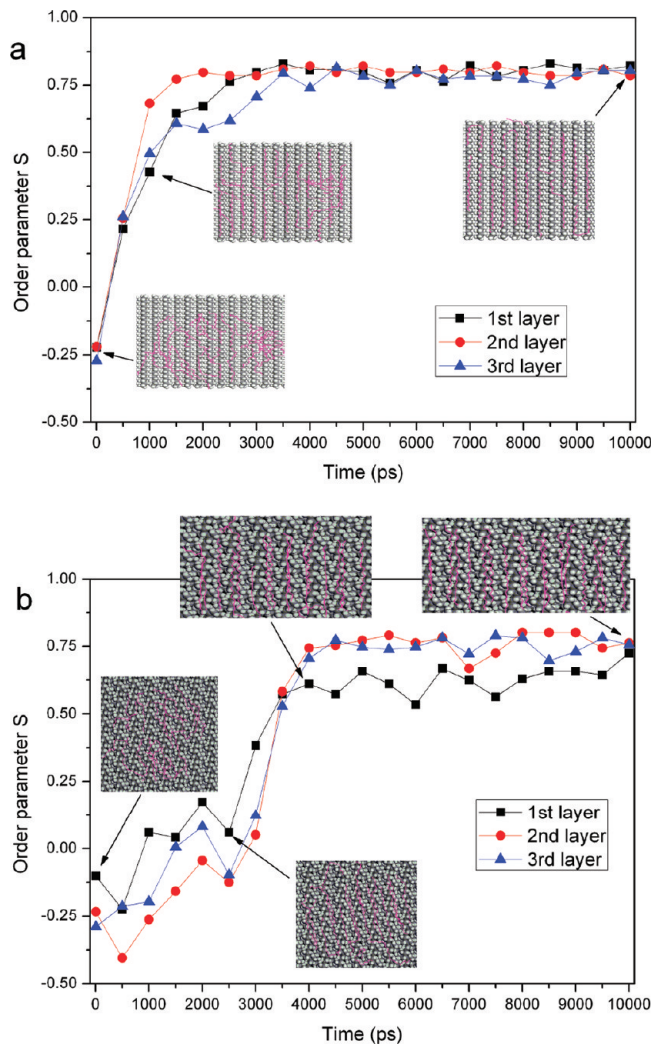


**Figure 5.** Bond-orientational order parameters  $S$  of the PE chains versus time: (a) PE/PES and (b) PE/PPS systems.

shish for polymer epitaxy or crystallization of kebab without flow. Figure 7 shows that the curves of the total potential energies still have a slight decrease after 2 ns, whereas no obvious decrease is observed after 4 ns. This finding implies that the 4 ns simulation time is long enough for our systems to reach a steady state. To observe the influence of the different surfaces, we calculated the polymer crystallization induced by the stretched PPB. The results in Figure 8 show that the PPB can induce polymer crystallization. By comparing Figure 8 with Figure 6, we can conclude that polymer crystallization depends on the structural similarity between the overgrowth polymer and the stretched polymer bundle. The ability of stretched bundles to induce polymer crystallization is stronger if they have a similar structure to that of the short polymer chains. Therefore, geometric matching should be the key factor for surface-induced polymer crystallization.

To understand further the mechanism of the polymer crystallization induced by the stretched bundle, we calculate the  $S$  values of the first three layers versus time. The results in Figure 9 show that the PE chains of the first three layers are parallel to the bundle direction and occur simultaneously, indicating that the stretched bundle of chains can certainly induce polymer crystallization without flow. This result is also consistent with the report of MuthuKumar et al.<sup>33</sup> and Liu et al.<sup>34</sup> that the kebab crystallization can grow in front of the crystal tip and does not necessarily need an external flow field. The comparison between parts a and b of Figure 9 shows that the PE chains need more time to adjust their configuration around the PPB. This result implies that the PPB has weaker ability to induce PE-chain crystallization, because the lattice match between the PE chains and PEB is better than that of PPB. Therefore, the lattice match should be an important factor for the surface-induced polymer crystallization.

In the polymer crystallization process, all the conformational changes of the backbone of the chains are relative to the freedom of the chains. Therefore, dynamic properties can also indicate the existence of polymer crystallization. In the molecular simulations, the dynamics of the PE chains around

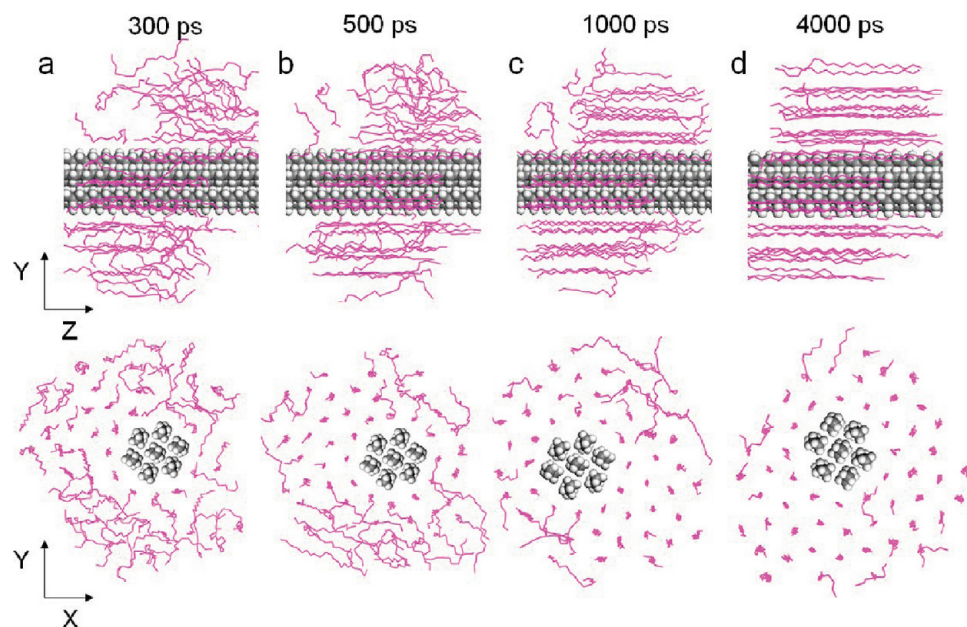


**Figure 6.** Snapshots of the atomic configurations of the PE melt induced by PEB.

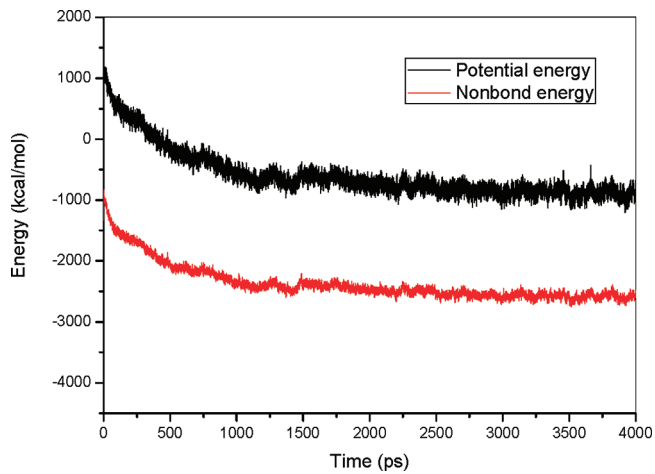


**Figure 7.** Time evolution of the nonbond and total potential energies of the PE/Peb system.

the polymer bundle can be described using the mean-square displacement (MSD)

$$\text{MSD}(t) = \langle r^2(t) \rangle \\ = \langle (1/N) \sum_{i=0}^N \sum_{X=x,y,z} |X_i(t) - X_i(0)|^2 \rangle \quad (6)$$

where  $X_i$  is the  $x$ -,  $y$ -, or  $z$ -coordinate of atom  $i$ ,  $N$  is the total number of atoms, and the angle bracket means averaging over the ensemble. Parts a and c of Figure 10 show the MSDs of all atoms for the PE bulk in the entire time region (1–4000 ps). After a long time, however, the plots deviated from linearity (Figure 10) because of the increasing statistical error involved in the calculations of MSD.<sup>35,36</sup> Notice that the MSD data presented above are calculated using all the three-dimensional coordinates, in which the anisotropies of the PE chains are not considered. To solve this problem, we calculate the MSDs of the PE chains along the three axes. This method is always used to solve the problem of the structural formation of polymer

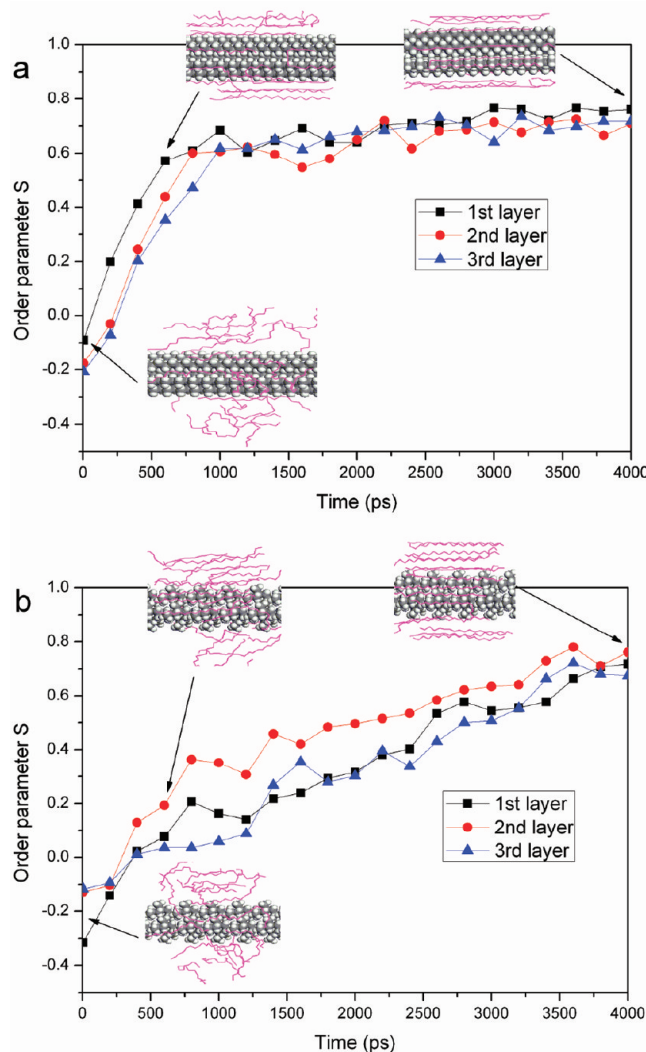


**Figure 9.** Bond-orientational order parameters  $S$  of the PE chains versus time: (a) PE/Peb and (b) PE/PPB systems.

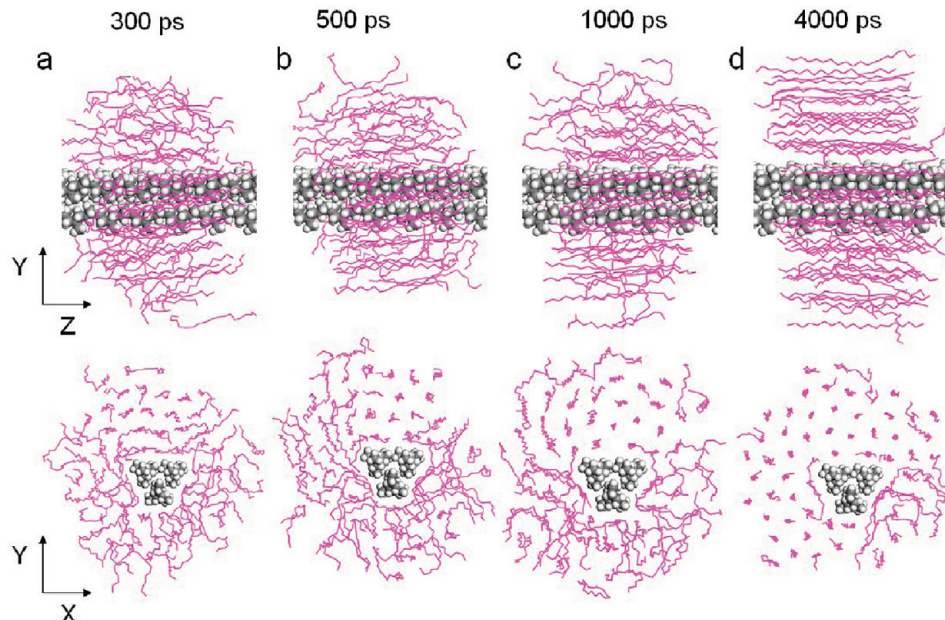


**Figure 8.** Snapshots of the atomic configurations of the PE melts induced by PPB.

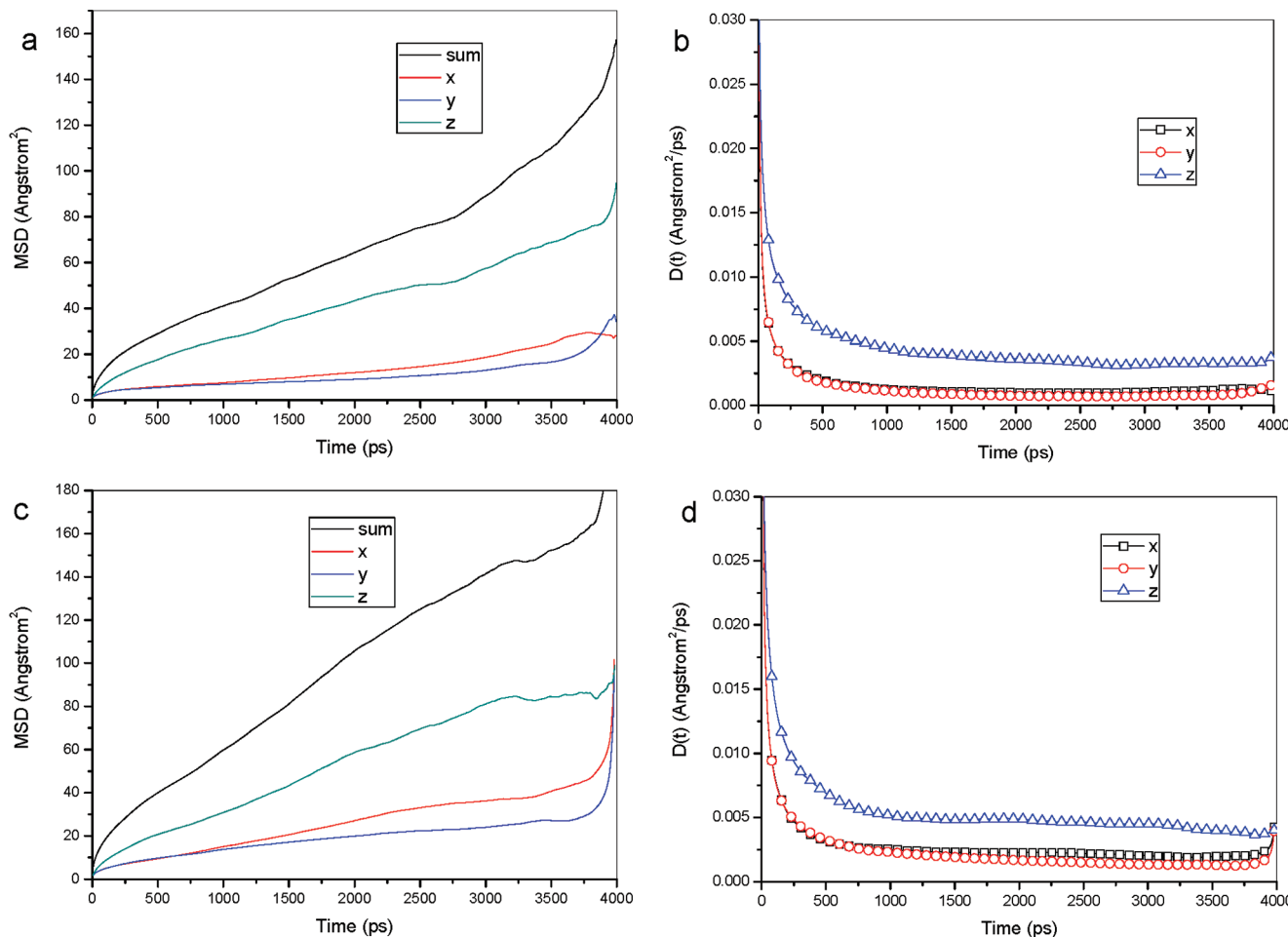


**Figure 10.** MSD and  $D(t)$  as a function of crystallization time for the PE chains: (a and b) PE/PEB and (c and d) PE/PPB systems.

chains influenced by the foreign surface.<sup>37</sup> Parts a and c of Figure 10 show that the MSDs along the  $x$ - and  $y$ -axes (2-D) are similar, particularly for the time region  $t \leq 1000$  ps. However, they were quite different from those along the  $z$ -axis (1-D). This result implies that the direction of the shish plays an important role in the crystallization of the kebabs.

The diffusion coefficient  $D$  of the PE chains has a more direct influence on the crystallization process. According to the Einstein equation,  $D$  can be considered constant and  $D(t)$  is the slope of the MSD versus time  $t$ .<sup>35</sup> Its values are  $0.38 \times 10^{-6}$  cm<sup>2</sup>/s and  $0.704 \times 10^{-6}$  cm<sup>2</sup>/s for PE/PEB and PE/PPB systems, respectively. By comparing the results of the PE/PEB system with those of the PE/PPB, we found that the PE chain has a larger  $D$  around the PPB than that of the PE around the PEB. However, Harmandaris et al. reported that  $D(t)$  is not constant in all cases.<sup>38</sup> Thus, we investigated the time-dependent diffusion coefficient,  $D(t) = \langle r(t)^2 \rangle / (6t)$ , of the PE chains.<sup>39</sup> Figure 10b and d shows the  $D(t)$  values along the three axes. As shown,  $D(t)$  suddenly drops after a very short period of time and then reaches a plateau. Among the three  $D(t)$  values, that of the  $z$ -axis is obviously larger than those of the  $x$ - and  $y$ -axes.

#### IV. CONCLUSIONS

In the current study, we performed the MD simulation of the isothermal polymer crystallization induced by the oriented polymer slab and the stretched polymer bundle. The simulation

revealed the ability of these materials to induce polymer crystallization, which is very difficult to resolve experimentally. Therefore, the current work provides unambiguous insight into the surface-induced polymer crystallization process. The results show that surface-induced polymer crystallization is greatly due to the interaction between the outer surface of the slab or bundle and the morphology of the random polymer chains.

The analyses on the S and MSD values show that the highly oriented slabs and the stretched bundle of PE are more efficient in inducing PE-melt crystallization than those of PP, implying that the structural similarity between the substrate and the overgrowth polymer in the contact lattice planes is a key factor for the surface-induced polymer crystallization.

#### ■ AUTHOR INFORMATION

##### Corresponding Author

\*Telephone: +86 535 6672870. Fax: +86 535 6672870. E-mail address: yangchuanlu@263.net.

##### Notes

The authors declare no competing financial interest.

#### ■ ACKNOWLEDGMENTS

The current work was supported by the National Science Foundation of China under Grant Numbers NSFC-10974078, NSFC-11174117, and NSFC-10674114.

**■ REFERENCES**

- (1) Ishida, H.; Bussi, P. *Macromolecules* **1991**, *24*, 3569–3577.
- (2) Russell, T. P.; Kumar, S. K. *Nature* **1997**, *386*, 771–772.
- (3) Lin, E. K.; Kolb, R.; Satija, S. K.; Wu, W. L. *Macromolecules* **1999**, *32*, 3753–3757.
- (4) Cao, Y.; Van Horn, R. M.; Tsai, C. C.; Graham, M. J.; Jeong, K. U.; Wang, B.; Auriemma, F.; De Rosa, C.; Lotz, B.; Cheng, S. Z. D. *Macromolecules* **2009**, *42*, 4758–4768.
- (5) Sun, Y.; Li, H.; Huang, Y.; Chen, E.; Gan, Z.; Yan, S. *Polymer* **2006**, *47*, 2455–2459.
- (6) Cheng, S.; Hu, W.; Ma, Y.; Yan, S. *Polymer* **2007**, *48*, 4264–4270.
- (7) Zhang, J.; Duan, Y.; Yan, S.; Yang, C.; Takahashi, I.; Ozaki, Y. *Macromolecules* **2010**, *43*, 5315–5322.
- (8) Jiang, S.; Qian, H.; Liu, W.; Wang, C.; Wang, Z.; Yan, S.; Zhu, D. *Macromolecules* **2009**, *42*, 9321–9324.
- (9) Kopp, S.; Wittmann, J. C.; Lotz, B. *Polymer* **1994**, *35*, 908–915.
- (10) Kopp, S.; Wittmann, J. C.; Lotz, B. *Polymer* **1994**, *35*, 916–924.
- (11) Xu, J. Z.; Chen, T.; Yang, C. L.; Li, Z. M.; Mao, Y. M.; Zeng, B. Q.; Hiso, B. S. *Macromolecules* **2010**, *43*, 5000–5008.
- (12) Yang, J. S.; Yang, C. L.; Wang, M. S.; Chen, B. D.; Ma, X. G. *Phys. Chem. Chem. Phys.* **2011**, *13*, 15476–15482.
- (13) Keller, A.; Kolnaar, H. W. H. *Flow Induced Orientation and Structure Formation*; VCH: New York, 1997; Vol. 18.
- (14) de Gennes, P. G. *J. Chem. Phys.* **1974**, *60*, 5030–5042.
- (15) Balzano, L.; et al. *Phys. Rev. Lett.* **2008**, *100*, 048302–048305.
- (16) Hsiao, B. S.; et al. *Phys. Rev. Lett.* **2005**, *94*, 117802–117805.
- (17) Zhao, B. J.; Li, X. Y.; Huang, Y. J.; Cong, Y. H.; Ma, Z.; Shao, C. G.; An, H. N.; Yan, T. Z.; Li, L. B. *Macromolecules* **2009**, *42*, 1428–1432.
- (18) Hu, W.; Frenkel, D.; Mathot, V. B. F. *Macromolecules* **2002**, *35*, 7172–7174.
- (19) Fujiwara, S.; Sato, T. *Phys. Rev. Lett.* **1998**, *80*, 991–994.
- (20) Accelrys Materials Studio 3.2; Accelrys Software, Inc.: San Diego, 2005.
- (21) Sun, H. *J. Phys. Chem. B* **1998**, *102*, 7338–7364.
- (22) Zheng, Q. B.; Xue, Q. Z.; Yan, K. Y.; Hao, L. Z.; Li, Q.; Gao, X. L. *J. Phys. Chem. C* **2007**, *111*, 4628–4635.
- (23) Yan, K. Y.; Xue, Q. Z.; Xia, D.; Chen, H. J.; Xie, J.; Dong, M. D. *ACS Nano* **2009**, *3*, 2235–2240.
- (24) Liu, W.; Yang, C. L.; Zhu, Y. T.; Wang, M. S. *J. Phys. Chem. C* **2008**, *112*, 1803–1811.
- (25) Grujicic, M.; Cao, G.; Roy, W. N. *Appl. Surf. Sci.* **2004**, *227*, 349–363.
- (26) Andersen, H. C. *J. Chem. Phys.* **1980**, *72*, 2384–2393.
- (27) Andersen, H. C. *J. Comput. Phys.* **1983**, *52*, 24–34.
- (28) Park, Y. J.; Kang, S. J.; Lotz, B.; Brinkmann, M.; Thierry, A.; Kim, K. J.; Park, C. *Macromolecules* **2008**, *41*, 8648–8654.
- (29) Cao, Y.; Van Horn, R. M.; Tsai, C. C.; Graham, M. J.; Jeong, K. U.; Wang, B.; Auriemma, F.; De Rosa, C.; Lotz, B.; Cheng, S. Z. D. *Macromolecules* **2009**, *42*, 4758–4768.
- (30) Yan, S. *Macromolecules* **2005**, *38*, 2739–2743.
- (31) Yan, S. *Polymer* **2006**, *47*, 2455–2459.
- (32) Sun, Y.; Li, H.; Huang, Y.; Chen, E.; Zhao, L.; Gan, Z.; Yan, S. *Macromolecules* **2005**, *38*, 2739–2743.
- (33) Dukovski, I.; Muthukumar, M. *J. Chem. Phys.* **2003**, *118*, 6648–6655.
- (34) Liu, T.; Lieberwirth, I.; Petermann, J. *Macromol. Chem. Phys.* **2001**, *202*, 2921–2925.
- (35) Charati, S. G.; Stern, S. A. *Macromolecules* **1998**, *31*, 5529–5535.
- (36) Ramírez, J.; Sukumaran, S. K.; Vorselaars, B.; Likhtman, A. E. *J. Chem. Phys.* **2010**, *133*, 154103–154114.
- (37) Wei, C. Y. *Phys. Rev. B* **2007**, *76*, 134104–134113.
- (38) Harmandaris, V. A.; Daoulas, K. C.; Mavrantzas, V. G. *Macromolecules* **2005**, *38*, 5796–5809.
- (39) Mitra, P. P.; Sen, P. N.; Schwartz, L. M. *Phys. Rev. B* **1993**, *47*, 8565–8574.